

A Novel Hydrogel Surface Grafted With Dual Functional Peptides for Sustaining Long-Term Self-Renewal of Human Induced Pluripotent Stem Cells and Manipulating Their Osteoblastic Maturation

Yi Deng, Shicheng Wei,* Lei Yang, Weizhong Yang,* Matthew S. Dargusch, and Zhi-Gang Chen

Realizing the clinical potential of human induced pluripotent stem cells (hiPSCs) in bone regenerative medicine requires the development of safe and chemically defined biomaterials for expansion of hiPSCs followed by directing their lineage commitment to osteoblasts. In this study, novel multipurpose peptide-presenting hydrogel surfaces are prepared on common tissue culture plates via carboxymethyl chitosan grafting and subsequent immobilization of two functional peptides allowing for in vitro feeder-free culture, long-term self-renewal, and osteogenic induction of hiPSCs. After vitronectin (VN) peptide modification, the engineered surfaces facilitate adhesion, proliferation, colony formation, and the maintenance of pluripotency of hiPSCs up to passage 10 under fully defined conditions without Matrigel or protein coating. Further, this synthetic niche exhibits an appealing regulatory effect on the osteogenic conversion of hiPSCs to osteoblastic phenotype without an embryoid body formation step by co-decoration of different ratios of VN and bone-forming peptide. Such a well-defined, xeno-free 2D engineered microenvironment not only helps to accelerate the clinical development of hiPSCs, but also provides a safe and robust platform for the generation of osteoblast-like cells or bone-like tissues at different maturation levels. Thus, the strategy may hold great potential for application in cell therapy and bone tissue engineering.

1. Introduction

Human induced pluripotent stem cells (hiPSCs) possess the prominent ability to self-renew and differentiate into a vast majority of specialized cells, displaying great potential for cell therapy and regenerative medicine.^[1] hiPSCs are an ideal cell source because they can be generated from human autologous somatic cells by a well-defined set of procedures which removes concerns regarding immune risks and ethical issues.^[2] Current approaches for culturing and expansion of hiPSCs rely on feeder cells layers (e.g., mouse embryonic fibroblasts,^[1c] human placental fibroblasts,^[3] and human foreskin fibroblasts,^[4] etc.) or animal/human-derived matrices (e.g., Matrigel^[5]) in conditional medium or commercial defined medium. Nevertheless, these animal- or human-derived cells and matrices bring about a myriad of critical problems associated with immunogenicity, microbial/viral contamination, chemically undefined and batch-to-batch

Dr. Y. Deng, Prof. S.-C. Wei
Central Laboratory
School and Hospital of Stomatology
National Engineering Laboratory for Digital and Material Technology of Stomatology
Academy for Advanced Interdisciplinary Studies
Peking University
Beijing 100081, China
E-mail: sc-wei@pku.edu.cn

Dr. Y. Deng, Prof. L. Yang, Prof. W.-Z. Yang
School of Chemical Engineering
School of Materials Science and Engineering
Sichuan University
Chengdu 610065, China
E-mail: ywz@scu.edu.cn

Prof. M. S. Dargusch, Prof. Z.-G. Chen
Materials Engineering
The University of Queensland
Brisbane, QLD 4072, Australia

Prof. M. S. Dargusch
Centre for Advanced Materials Processing and Manufacturing (AMPAM)
School of Mechanical and Mining Engineering
The University of Queensland
Brisbane, QLD 4072, Australia

Prof. Z.-G. Chen
Centre for Future Materials
The University of Southern Queensland
Springfield, QLD 4300, Australia

 The ORCID identification number(s) for the author(s) of this article can be found under <https://doi.org/10.1002/adfm.201705546>.

DOI: 10.1002/adfm.201705546

inconsistency in quality, which severely hampers the clinical adaptation of hiPSCs.^[6] Over the decades, a number of engineered substrates were coated with proteins (e.g., vitronectin (VN),^[7] laminin,^[8] and fibronectin,^[9] etc.), protein fragments (e.g., laminin E8 fragments^[10]), and cell adhesion molecules (e.g., recombinant E-cadherin^[11]), which provide artificial extracellular matrix (ECM)-like microenvironments to maintain proliferation and self-renewal of human pluripotent stem cells (hPSCs, including hiPSCs and human embryonic stem cells (hESCs)) under xeno-free conditions.^[12] Nevertheless, the high cost of culturing hiPSCs is remarkably influenced by the use of these biological matrices, imposing a great obstacle for large-scale cultivation of hiPSCs to acquire adequate cell numbers for clinical applications. Therefore, establishing chemically defined, economical, scalable synthetic surfaces for hiPSC expansion is indispensable for production of clinical grade hiPSCs and fundamental research.

In terms of clinical bone regenerative therapies, transplantation of autologous grafts is the current “gold standard” of bone substitution, but it also has numerous inherent limitations such as donor site morbidity, available quantities, and host immune rejection.^[13] Cell therapy based on hiPSCs opens up a new avenue and opportunity for complex bone loss treatments. Despite of the advantages mentioned above that hiPSCs offer directing their differentiation into bone-functional cells remains a significant challenge. Several studies reported in the literature have showed that fibrous scaffolds (e.g., poly(L-lactic acid)^[14] and poly(ether sulfone)^[15] fibers) can efficiently enhance the differentiation of embryoid bodies (EBs) into osteoblastic lineage in osteoinductive medium. EBs are commonly adopted for the differentiation of hPSCs because they mimic the three dimensionalities of development during gastrulation and formation of the three germ layers in vivo. Nonetheless, the limitation of employing EBs for differentiation studies arises from the fact that the yield of desired cells is much lower than the initial amount of cells.^[13] Karp et al. have confirmed that the formation of EBs prior to chemically induced osteogenic differentiation is not necessary^[13] and may, in fact, hamper the osteogenic potential of hPSCs.^[16] Some osteomimetic polymer scaffolds were recently developed to induce osteogenic commitment of hPSCs without the step of EBs formation.^[17] This approach, however, requires a Matrigel or ECM protein precoat on the materials' surface in order to assist with the initial attachment of the hPSCs. We are curious as to whether it is feasible to control osteogenic differentiation of hiPSCs without both Matrigel coating and EBs formation.

Peptide presenting substrates, exhibiting comparable capabilities in supporting adhesion and self-renewal of hPSCs to that of Matrigel coating, are considered as one of the most promising approaches for large scale expansion and differentiation of hPSCs under chemically defined conditions.^[18] A RGD-containing oligopeptide derived from VN has been shown to support the successful proliferation and self-renewal of hPSCs for >20 successive passages.^[18a,19] Another peptide, bone forming peptide (BFP) from bone morphogenetic protein-7 (BMP-7), demonstrated by Kim et al.^[20] had greater osteogenic activity than BMP-7 and induced osteogenesis of human mesenchymal stem cells.

Our previous work indicated that BFP peptide has an obvious enhancement function on the osteogenic conversion of hPSCs.^[21] Accordingly, we hypothesize that the two functional peptides grafted on the tissue culture plate (TCP) will sustain the proliferation of hiPSCs at the initial stage of growth and stimulate their osteogenic commitment later. Furthermore, by regulating the VN/BFP ratios on the engineered surface it is possible to obtain different maturity levels of the osteoblast-like cells. In order to firmly immobilize peptide onto TCP, an assisted carboxymethyl chitosan (CMC) layer should be introduced. Compared with other glycosaminoglycans, carboxymethyl chitosan (CMC), a water-soluble chitosan derivative, is a natural linear amino-polysaccharide with a large number of amine and carboxyl groups. With nonimmunogenicity, biodegradability, excellent biocompatibility, and intrinsic antibacterial properties, CMC finds a wide range of applications in biomedical field.^[22] Simultaneously, CMC can enable to induce osteogenic differentiation of cells owing to the structural similarity to glycosaminoglycans in ECM.^[23] CMC as a bridge is grafted onto TCP surface through the formation of a thin hydrogel, and the residual carboxyl groups are used for tethering a large amount of peptide. Herein, the aims of the present work are: (1) to develop and characterize the hydrogel surface which has been co-decorated with dual functional peptides on TCP (VN/BFP–TCP); (2) to investigate its role in supporting survival and maintaining pluripotency of hiPSCs for long-term passages; (3) to assess in vitro the osteogenesis ability of hiPSCs on the functional surfaces that had been co-decorated with dual peptides and various VN/BFP ratios. We believe that our strategy has great potential for application in bone regenerative medicine and cell therapy.

2. Results and Discussion

2.1. Preparation and Characterization of the Novel Hydrogel Surface After Grafting with Peptides

We developed a novel VN peptide-grafted hydrogel surface for the survival and long-term culture of hiPSCs as shown in **Figure 1**. The TCP substrate is firstly treated under UV-ozone conditions to generate polar groups (–COOH, –OOH, –C=O) on the surface for better immobilization of the biomolecules before CMC is deposited on the activated surface to act as a bridge (intermediate layer). The –COOH and –NH₂ groups in the CMC macromolecules are cross-linked to form hydrogel through the *N*-hydroxysuccinimide (NHS)/*N'*-ethylcarbodiimide hydrochloride (EDC) chemistry, and the terminal –COOH on the hydrogel surface synchronously reacts with the –NH₂ groups from the VN peptide, producing peptide tethering surfaces for the culture of hiPSCs without a Matrigel coating.

The chemical compositions and morphologies of the peptide-presenting substrates were characterized by contact angle goniometry, attenuated total reflectance-Fourier transform infrared spectroscopy (ATR-FTIR), X-ray photoelectron spectroscopy (XPS), scanning electron microscope (SEM), as well as atomic force microscopy (AFM). The water contact angle

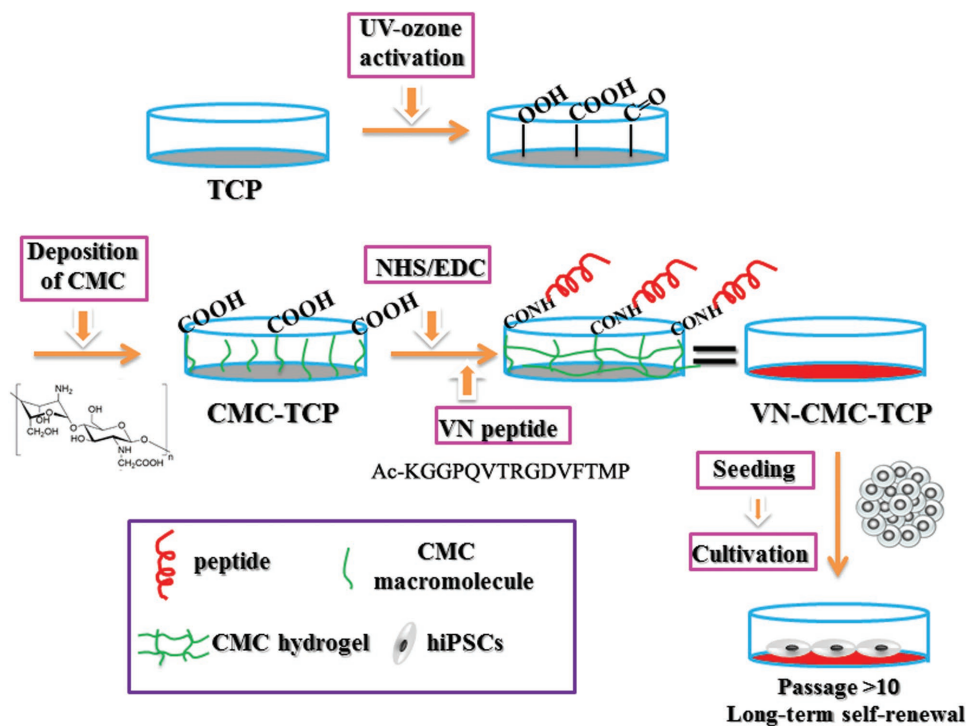


Figure 1. Schematic illustration of the preparation of peptide-grafted hydrogel microenvironment for long-term self-renewal of hiPSCs.

is indicative of the effectiveness of the surface modification protocols. As depicted in **Figure 2a**, a pristine TCP dish has a contact angle of $\approx 63^\circ$ (relatively hydrophobic), which decreases to an average value of 34.6° after the coating of CMC. This is likely due to the presence of the hydrophilic groups ($-\text{OH}$, $-\text{COOH}$, and $-\text{NH}_2$) in the grafted CMC. After immobilizing peptide onto the CMC-modified surface, the contact angle continuously reduces to about 14.6° , which can be attributed to the superhydrophilic nature of the peptide. Next, ATR-FTIR spectra (**Figure S1**, Supporting Information) shows that in addition to the peak of H_2O at 3462 cm^{-1} , the adsorption bands at 1564 and 1447 cm^{-1} are assigned to the stretching vibrations of $-\text{NH}_3^+$ and $-\text{COO}^-$,^[24] respectively, which are the characteristic peaks of CMC. After peptide modification, the new peaks at 1650 and 1533 cm^{-1} are clearly observed. These are associated with the deforming vibration of amide I ($\delta\text{N}-\text{H}$) and stretching vibration of amide II ($\nu\text{C}=\text{O}$) from the peptide,^[25] suggesting that the VN peptide is effectively bonded onto the TCP substrates via the CMC interlayer.

These findings were further confirmed by XPS survey scans (**Figure 2b**, **Figure S1** and **Table S3**, Supporting Information). Carbon and oxygen elements are the predominant components of the pristine TCP substrates. Successful anchoring of CMC is indicated by an increase in the N 1s and O 1s content, and a corresponding decrease in the C 1s content from 87.96% to 76.76% is shown in **Table S3** in the Supporting Information. Upon attachment of peptide, notably in the wide-scan spectra, the appearance of a sodium signal (because peptide is dissolved in PBS buffer), and the enhancement of N 1s (from 6.65% to 11.91%) on the surface of VN-CMC-TCP samples indicates successful tethering of the VN peptide. Furthermore, an evident change in the carbon

bond composition observed in the high-resolution narrow carbon spectra (C 1s) clearly supports these conclusions (**Figure S1b-d**, Supporting Information). The high-resolution C 1s spectrum of the pristine TCP shows that the binding energies centered at 284.7 , 285.8 , and 291.6 eV are assigned to the $-\text{C}-\text{C}-/\text{C}-\text{H}-$, $-\text{C}-\text{OH}$, and $-\text{O}-\text{C}=\text{O}$ bonds, respectively. After CMC coating, the intensity of the carbon skeleton ($-\text{C}-\text{C}-/\text{C}-\text{H}-$) decreases dramatically, and the peaks of the hydroxyl ($-\text{C}-\text{OH}$) and carbonyl ($\text{C}=\text{O}$) groups increase as shown in **Figure S1c** in the Supporting Information. This should be attributed to hydrophilic groups of CMC. Whereas a broad peak of the $-\text{C}-\text{N}-$ bond at about 285.2 eV is newly recorded on both CMC-TCP and VN-CMC-TCP samples, indicating the presence of CMC and peptide. Compared with that of CMC-TCP, the peaks of $-\text{C}-\text{N}-$ and $\text{C}=\text{O}$ for VN-CMC-TCP are enhanced greatly in intensity due to the abundant presence of amine and amide bonds ($-\text{NH}-\text{C}=\text{O}$) in the structure of peptide. Furthermore, by fitting the distribution of the high-resolution N 1s spectra of CMC-coated and peptide-grafted TCP using a Gaussian/Lorentz curve (**Figure S1e,f**, Supporting Information). The peaks centered at 399.6 , 400.2 , and 401.8 eV are consistent with the amine bond ($\text{R}-\text{NH}_2$), amide ($-\text{NH}-\text{C}=\text{O}$), and protonated amine specie ($\text{R}-\text{NH}_3^+$), respectively. The $-\text{NH}-\text{C}=\text{O}$ component appears accompanied the reduction of $\text{R}-\text{NH}_2$ and $\text{R}-\text{NH}_3^+$ in the spectrum of the VN-CMC-TCP sample, which may be attributable to formation of the covalent bonding between the negative COO^- group of CMC and the $\text{R}-\text{NH}_2$ group of the peptide. These results further demonstrate successful conjugation of VN peptide to the TCP surfaces.

The surface morphology and roughness of the TCP substrates were altered by CMC and peptide

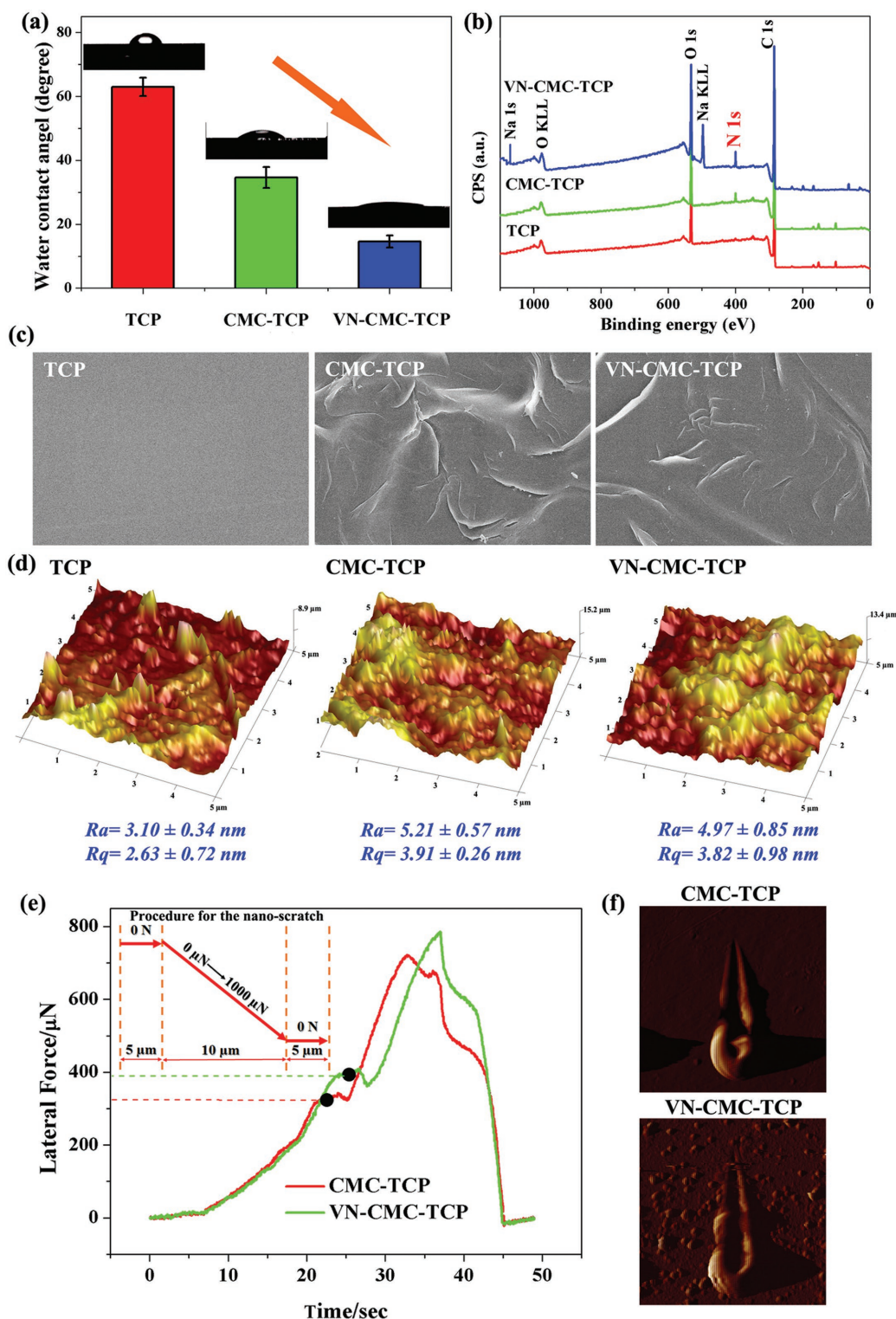


Figure 2. Surface characterization of VN peptide/CMC functionalized TCP substrates. a) The alteration of contact angles during each step of the VN–CMC–TCP surface coating process. Corresponding images of water droplet on sample surfaces have also been presented. The hydrophilicity is significantly enhanced after CMC/VN peptide modification. b) XPS analyses and of the bare TCP, CMC–TCP, VN–CMC–TCP substrates. Surface topologies of these substrates were examined by c) SEM and d) AFM. Surface roughness including Ra and Rq were determined from the AFM roughness profiles. e) Lateral forces change with time during the nano-scratch resistance tests. The insert at the upper left corner shows the steps for the nano-scratch resistance test. Black dots signify the critical point of the lateral force. f) Post-test surface morphologies of the samples after sequential modification by the CMC/VN peptide are recorded.

immobilization. SEM images (Figure 2c) shows that pristine TCP displays a smooth surface, while the wrinkled CMC membrane is observed on the CMC–TCP and VN–CMC–TCP surfaces. AFM analysis (Figure 2d) further confirms the SEM results, that Ra and Rq of the modified surfaces are larger than those of the unmodified TCP surface, indicating that the coating of CMC and peptide enhances the surface roughness of the TCP substrate. Nano-indentation is a popular technique to detect microscale surface mechanical properties; particularly because it provides a simple and rapid means to assess the scratch-resistance of the coated films.^[26] The critical lateral force at the coating failure in the ramp-load scratch steps is in positive correlation with the adhesion strength of the coating, and the data is shown in Figure 2e. The critical lateral force required for initiating coating failure for VN–CMC–TCP is higher than that for CMC–TCP, i.e., 398 μN at 26 s for VN–CMC–TCP versus 315 μN at as early as 21 s for CMC–TCP, indicating stronger adhesion. The strong adhesion between the CMC/peptide coating and the TCP substrate can be attributed to the strong intermolecular hydrogen bonding and electrostatic interaction between them. The spallation of the coating under the critical load condition is shown in Figure 2f, and the depth of the scratch on the VN–CMC–TCP seems to be more superficial than that of CMC–TCP substrate, indicating better elastic resilience of the CMC/peptide coating, which results in the ability to better maintain the integrity as well as durability of the coating.

2.2. CMC and VN Peptide Densities Influence hiPSCs Proliferation

Previous studies have demonstrated that peptide density on the material surface played an important role in cell responses.^[18c,27] To investigate the influence of peptide and CMC densities on the cell number and morphology, hiPSCs were seeded onto the surfaces that had been treated with various ligand concentrations. As shown in Figure 3a, cell numbers display an analogous Gaussian distribution with CMC concentration increasing. The peak of cell number occurs at 3% CMC concentration, then the amount of cells significantly reduces to about 0 when the CMC concentration is increased to 10%. This is probably because the lower CMC concentration provides inadequate carboxyl group for peptide tethering, contributing to reduced cell number. While higher CMC concentration tends to form a thicker hydrogel, and hiPSCs are easily entrapped into the hydrogel, which is not beneficial to promote culture and adhesion of hiPSCs.

A good correlation is observed between conjugated peptide density and hiPSCs numbers after 1 d on the VN-presenting substrate as show in Figure 3b. On the basis of the calculations, peptide density on the VN–CMC–TCP surface is enhanced with VN peptide concentration (Figure S2, Supporting Information), and there is a sustained increase in cell numbers as the peptide concentration increasing from 0 to 1.25×10^{-3} M. When peptide concentrations are 1 and 1.25×10^{-3} M, cell numbers on the substrate are about 80% of that on the Matrigel, and there is no significant

difference in cell numbers between the 1 and 1.25×10^{-3} M groups because of similar peptide density at about 15 pmol mm^{-2} on the two surfaces (Figure S2, Supporting Information). Figure 3c shows that no hiPSCs adhesion is observed on the surface of the samples with 0×10^{-3} M peptide concentration. At low peptide concentrations (0.25 – 0.75×10^{-3} M), although a small amount of hiPSCs colonies attach to the surface, they appear as poorly spread clusters of cells surrounded by multiple areas of differentiated cells with rough colony borders. Their morphologies are highly variable, and some colonies exhibit loose borders between cells, while others did not (Figure 3c). Above 0.75×10^{-3} M, the hiPSCs exhibit morphologies very similar to undifferentiated hiPSC on the Matrigel-coated surface, with compact colonies and a smooth colony border. In addition, uniform distribution of the hiPSC colonies implies uniformity of the peptide on the surfaces. We next seeded hiPSCs onto VN–CMC–TCP (3% CMC + 1×10^{-3} M VN peptide) and Matrigel-coated surface as a single cell, and the cell attachment process was investigated by live cell images at time intervals of 1, 3, 12, and 24 h (Figure S3, Supporting Information). A large number of single cells attach on both surfaces at initial 1 h. When cultured for 3 h, more well-spread out and migrated hiPSCs are observed on the Matrigel-coated surface. Then, hiPSCs colonies with similar size are found on both the Matrigel and VN-displaying surfaces after 12 and 24 h of seeding, indicating that with the help of Rock inhibitor (an inhibitor of dissociation-induced apoptosis),^[28] cell adhesion on VN–CMC–TCP surfaces is similar to that on Matrigel coated surfaces, which is a golden standard for the hPSCs culture. These results indicate that the combination of 3% CMC and 1×10^{-3} M peptide on the surface is an optimal parameter to permit normal growth and expansion of hiPSCs.

2.3. Long-Term Culture of hiPSCs on VN Peptide-Grafted Hydrogel Surfaces

To assess the ability of the VN peptide-grafted hydrogel surface to support the long-term self-renewal of hiPSCs, hiPSCs were serially cultured on the substrate for ten passages in a xeno-free commercial defined medium (mTeSR1), and several characteristics were studied: colony morphology, cell viability, and the expression of hiPSCs biomarkers. As depicted in Figure S4 in the Supporting Information, the cells continuously maintain typical undifferentiated morphology and grow in colonies on the VN peptide-grafted substrate, as characterized by compact colonies with defined edges and large nuclei-to-cytoplasm ratios, similar to that on Matrigel control. Studies on the growth curve of hiPSC on the hydrogel and Matrigel surfaces were conducted for 1 week via CCK-8 assay. It is obvious that the OD value increases with time through p1, p5, and p10, indicating that the peptide-grafted substrate supports hiPSC proliferation. Furthermore, the proliferation rate on the VN–CMC–TCP surface is similar to that on the Matrigel-coated surface at each passage, although there is little difference in cell viability between two groups at certain times. The CCK-8 assay demonstrates that through multiple generations, the hiPSCs still retain good proliferation on the VN peptide-presenting TCP.

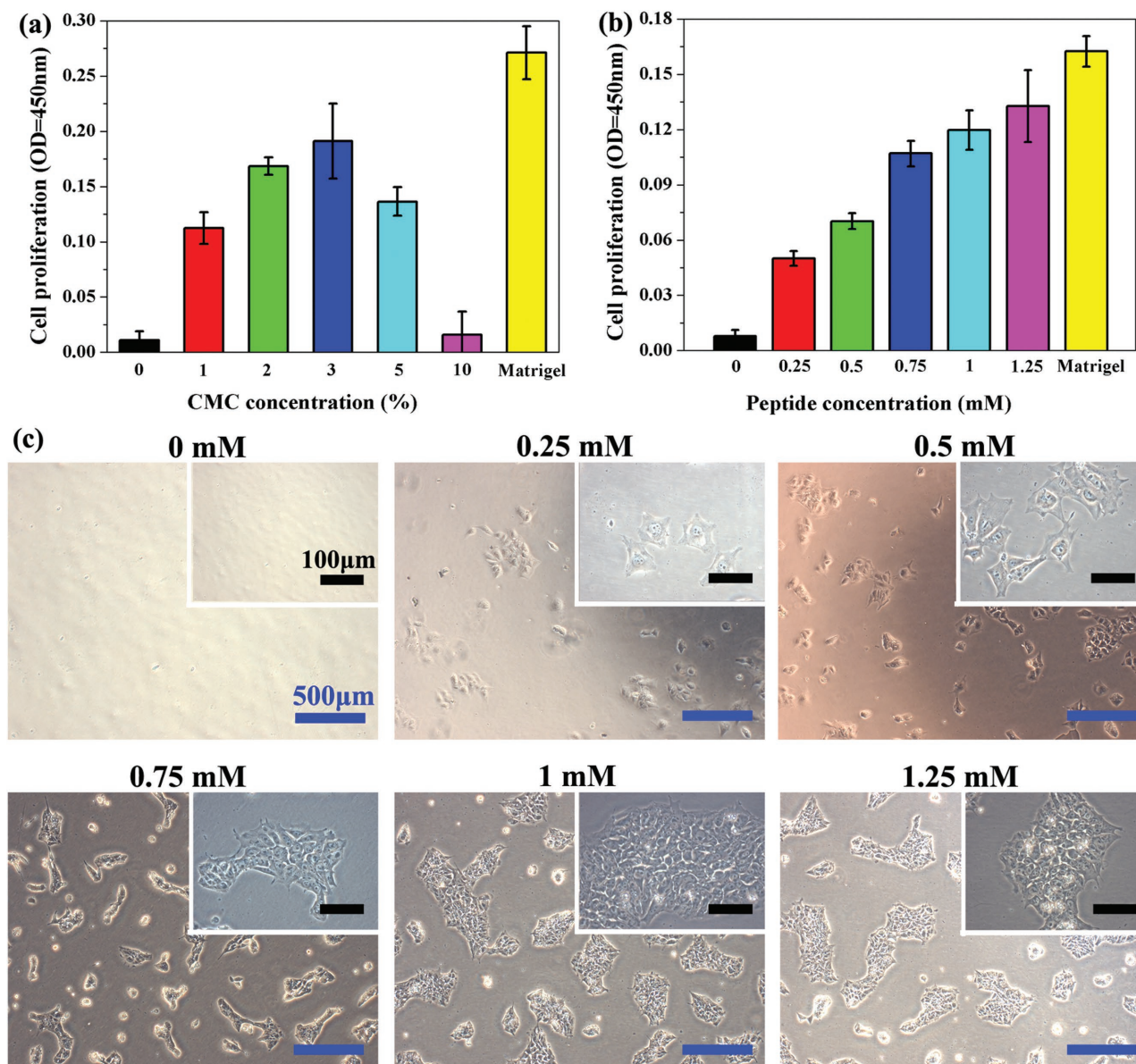


Figure 3. Cell attachment and survival on various VN-presenting surfaces. a) CMC concentration-dependent and b) peptide concentration-dependent attachment of hiPSCs. c) Phase-contrast images of hiPSCs morphologies on the VN-CMC-TCP surfaces with different peptide concentrations. Images at the upper right corner show an enlarged view of hiPSCs colonies. Scale bars: blue 500 μ m; black 100 μ m.

Maintenance of pluripotency is a critical parameter when evaluating new surfaces for hiPSC culture. Immunofluorescence staining was carried out to assess whether cells retained markers of undifferentiated hiPSC. Results show the strong positive staining of Nanog, Oct-4, SSEA-3, SSEA-4, and Tra-1-60 in cultures of the VN peptide-grafted hydrogel surface throughout p1, p5, and p10 (Figure 4b). To quantify the pluripotency expression of the cells, three pluripotent markers (Nanog, Oct-4, and Sox-2) were selected for use in real-time polymerase chain reaction (RT-PCR) analysis. The data reveals that the hiPSCs cultured on the VN peptide-grafted substrate express similar levels of the pluripotent markers to those on the Matrigel group, verifying that the hiPSC robustly maintain their undifferentiated characteristics very well on the hydrogel substrate for long-term passages.

The quantitative expressions of Oct-4, Nanog, SSEA-3, and Tra-1-60 in hiPSCs colonies cultured on VN peptide-presenting hydrogel and Matrigel-coated surfaces were further assessed for ten passages (Figure 5b). Although there are fluctuations, the cells on VN-CMC-TCP surfaces express a similar level of Oct-4 and SSEA-3 to those of Matrigel cultures, proving that the pluripotency of hiPSCs cultured on VN-CMC-TCP surfaces are comparable to those produced using the Matrigel control. In addition, at p1, p5, and p10 passages, fluorescence activating cell sorter (FACS) analysis indicates that more than 93.4% and 98.4% of hiPSCs grown on VN-CMC-VN surfaces are positive in Nanog and Oct-4 expression, respectively, through ten passages (Figure 5d). Moreover, we also measured the expression of SSEA-3 and Tra-1 60 for hPSCs grown on

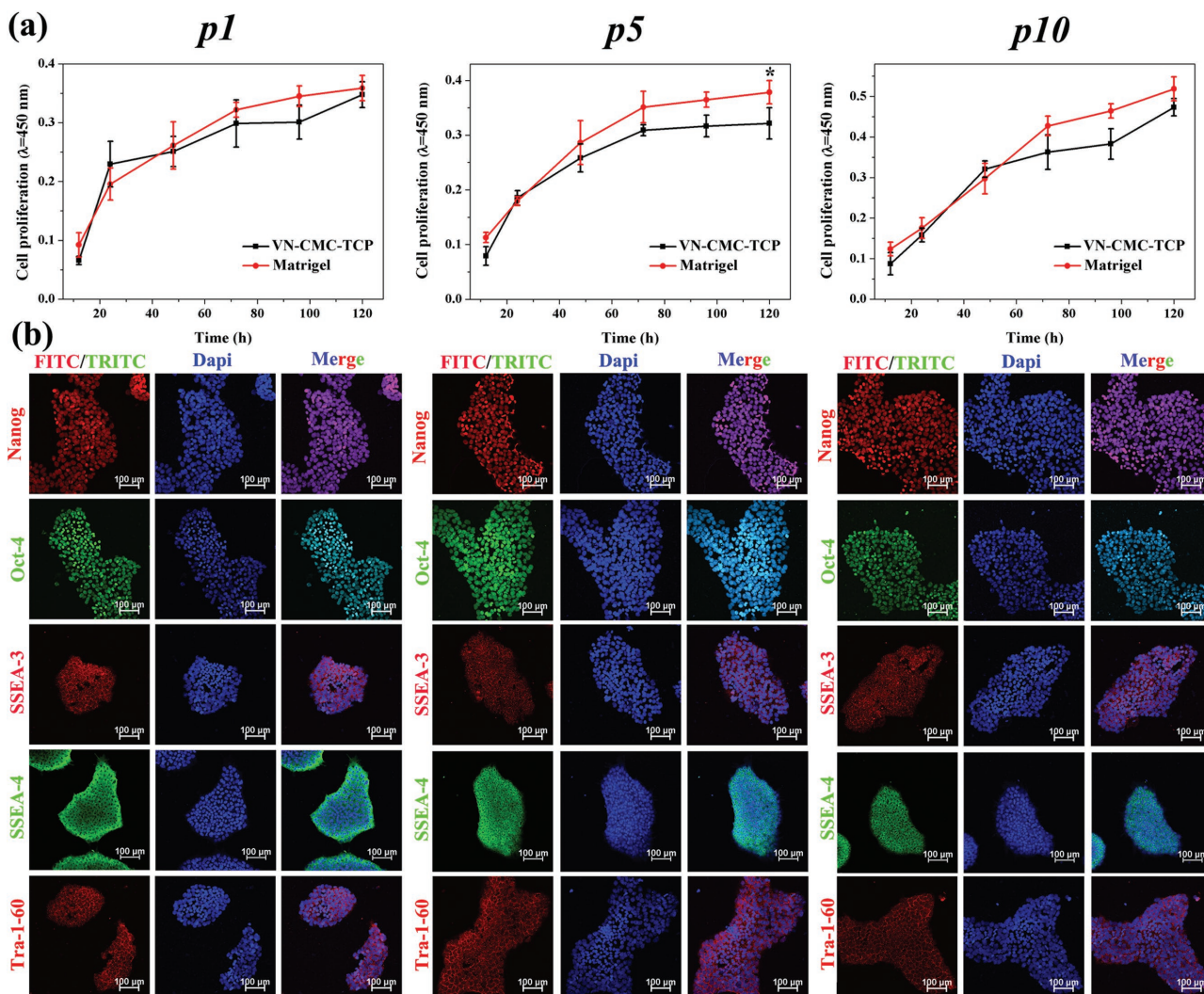


Figure 4. a) Cell proliferation evaluation of hiPSCs over the course of ten passages on VN-CMC-TCP surfaces. b) Immunocytochemical staining of pluripotency biomarkers including Nanog (red), Oct-4 (green), SSEA-3 (red), SSEA-4 (green), and Tra-1-60 (red) in hiPSCs cultured on the VN peptide-grafted hydrogel surface for p1, p5, and p10 in mTeSR1 medium. Nuclei are visualized by Dapi-staining (blue). Scale bars: 100 μm . *: $p < 0.05$ versus Matrigel.

VN-CMC-VN surfaces at p1, p5, and p10 using FACS too. At least 86.1% of these cell samples positively express SSEA-3, and 96.0% for Tra-1 60. In addition at each passage (p1, p5, and p10), their karyotypes remain intact (Figure 5e). Overall, the results demonstrate that a short peptide sequence of VN protein conjugated on the CMC-modified surface is sufficient to support long-term self-renewal of hiPSC under a fully defined medium.

2.4. Osteogenic Differentiation of hiPSCs on the Hydrogel Surface that Had Been co-Decorated with Dual VN/BFP Peptides

Even though it is clear that the aforementioned method is successful in decorating the VN and BFP peptides on the modified TCP surfaces; afterward, it is also important to determine whether they are immobilized at the presupposed volume ratios. Figure 6a shows that the uniform fluorescence

distribution is observed in different experimental groups, showing the homogeneity of peptides on the surfaces. The intensity of green light (VN) gradually decreases, and red light (BFP) gradually increases on the treated samples, which suggest that the VN and BFP-1 peptides are successfully immobilized at the designed ratios. The trend of fluorescence intensity was further confirmed by the results of quantification presented in Figure 6b. According to the calculations, when reacted with pure VN solution, approximately $14.50 \pm 2.56 \mu\text{g cm}^{-2}$ VN is immobilized on the VN₁₀-TCP plates. VN densities in VN₈/BFP₂-TCP, VN₅/BFP₅-TCP, and VN₂/BFP₈-TCP yield 11.61 ± 1.46 , 6.75 ± 1.39 , and $2.31 \pm 1.07 \mu\text{g cm}^{-2}$ respectively, and corresponding BFP densities in the three substrates are 3.16 ± 0.99 , 5.68 ± 2.69 , and $9.78 \pm 3.68 \mu\text{g cm}^{-2}$, respectively.

In order to examine the influence of the introduction of BFP peptide on cell propagation and growth of hiPSCs, an additional experimental investigation was conducted. Obviously, there is a

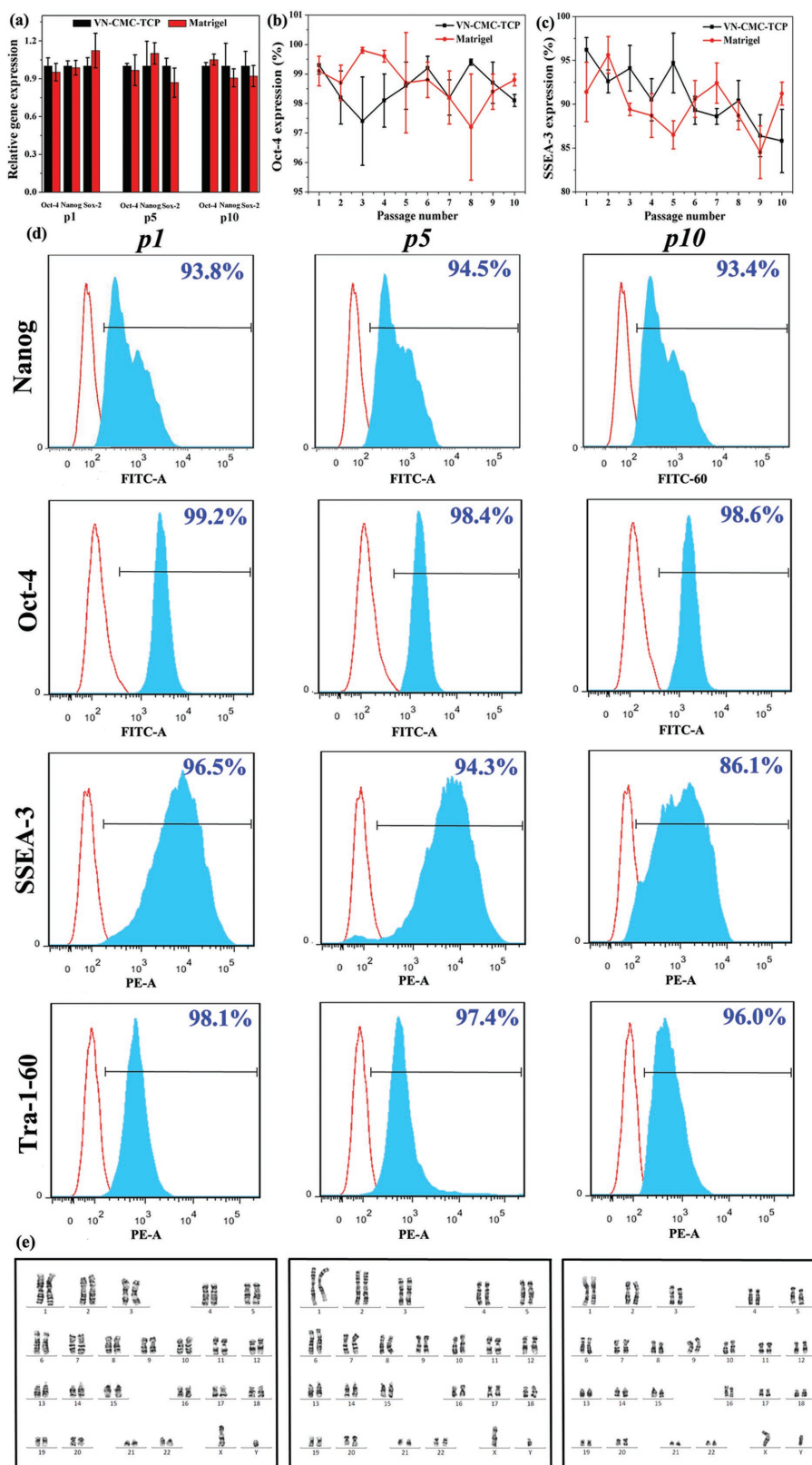


Figure 5. a) Quantitative RT-PCR analysis for examining the pluripotency maker expression (Oct-4, Nanog, and Sox-2) in hiPSCs at p1, p5, and p10 cultured on VN-CMC-TCP and Matrigel surfaces. b) Oct-4 and c) SSEA-3 expressions of hiPSCs cultured on VN-CMC-TCP and Matrigel surfaces for ten sequential passages measured by FACS. d) FACS analysis of Nanog, Oct-4, SSEA-3, and Tra-1-60 and e) Karyotype analysis for hiPSCs on VN-CMC-TCP surface at p1, p5, and p10. IgG and IgM control: unfilled red peak; FITC or PE-conjugated antibody: filled blue peak.

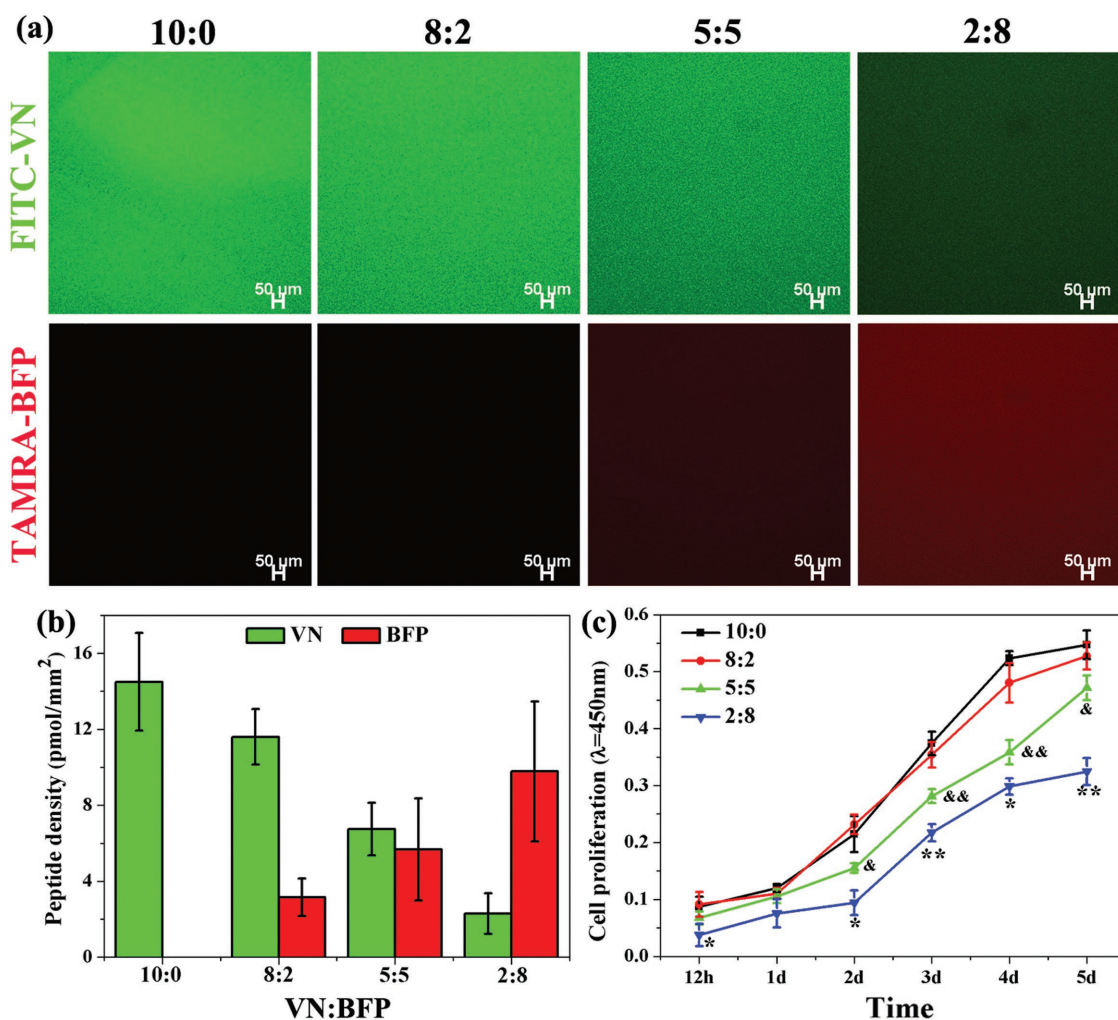


Figure 6. a) Visualization of fluorescently labeled peptides (FITC–VN peptide and TRITC–BFP peptide) and b) Quantitative peptide intensity immobilized on the dual VN/BFP peptide-decorated TCP surfaces with different ratios ($n = 6$). c) Cell proliferation of hiPSCs cultured on the substrates that had been co-decorated with dual VN/BFP peptides are evaluated using the CCK-8 assay at specific time intervals ($n = 6$). *: $p < 0.05$ and **: $p < 0.01$ versus other groups, &: $p < 0.05$ and &&: $p < 0.01$ versus VN₁₀/BFP₀ and VN₈/BFP₂ groups.

correlation between VN/BFP ratio (i.e., conjugated VN peptide density) and hiPSCs numbers during the 5 d of culture. The cell numbers are enhanced with increasing VN peptide concentrations on the TCP substrates that has been co-decorated with dual peptides, because more VN peptides contribute to an increase in the larger number of sites for cell anchoring, consistent with earlier studies.^[6b,18c] At 7 d, the numbers of cells on the VN₅/BFP₅-TCP, VN₈/BFP₂-TCP, and VN₂/BFP₈-TCP surfaces are about 96.4, 86.2, and 59.3% of that on the VN₁₀-TCP surface, respectively. By 7 d of culture, hiPSCs on the matrices grow to reach confluence, except on the VN₂/BFP₈-TCP surface, indicating that the introduction of BFP peptide at a certain concentration has no impact on proliferation and growth of hiPSCs, and these surfaces still provided abundant cells for osteogenesis.

In order to the realization of the clinical potential of hiPSCs in bone regenerative medicine, it is much-needed to design an osteogenic microenvironment that mimics niche cells and induces ossification on chemically defined surfaces. The

hiPSCs on the hydrogel surfaces that had been co-decorated with dual peptides were cultured in osteoinductive media. In order to evaluate whether the hiPSCs are directly induced toward osteogenic lineages in vitro, the cellular morphological alteration, alkaline phosphatase (ALP) activity, and calcium nodule deposition, expression of osteogenesis-related genes, as well as corresponding protein expression were assessed at specific time intervals.

Before osteogenic induction, hiPSCs colonies maintain their intrinsic undifferentiated morphology, while after directed differentiation in osteoinductive media, apparent changes in cell morphology are observed. From the optical images, the cell colonies collapse, and differentiated cells with well-spread morphology migrate from the periphery of the hiPSCs colonies at 4 d. Interestingly, some nodules appeared after 21 d of osteogenic stimulation can be the calcium mineralization products (Figure 7a). SEM images also confirm that cell colonies collapse to single cells, possessing a low degree of cell–cell contact. As time progressed,

they display a highly fusiform morphology with numerous filopodia, similar to osteoblastic shapes reported in previous work,^[29] demonstrating good adhesion and spreading of cells. In addition to cellular morphological alteration, most differentiated cells seeded on hydrogel samples that had been co-decorated with dual peptides exhibit favorable spreading by reorganizing the focal adhesions and filamentous F-actin, quite different from that observed on the undifferentiated hiPSCs (Figure 7c).

ALP, an early marker of osteogenesis, is strongly expressed in the undifferentiated hPSCs, as well as in the osteoblasts.^[30] As shown in **Figure 8**, initially hiPSCs express high ALP activity in the range of 70–95 U g_{prot}⁻¹, suggesting that the hiPSCs maintain good pluripotency. Afterward, the production of ALP sharply decreases to about zero after being induced for 4 d, indicating that hiPSCs lose their stem cell properties. Later, the expression of ALP stably increases and maintains at a high value after 14 d. The re-expression of ALP signifies the appearance of osteogenic progenitors after 14 d of osteoinductive culture. It is notable that the highest amount of ALP expression is detected on the VN₅/BFP₅-TCP surface, and the cells on the VN₈/BFP₂-TCP substrate induce the lowest ALP activity due to low number of cells on the surface. These results were further qualitatively verified via enzyme-histochemistry (EHC) staining of ALP at 21 d (Figure 8b), which shows a good material-dependent ALP expression. By comparison, the ALP-positive areas are obviously larger and more purple on the VN₅/BFP₅-TCP substrates than those on the other substrates, suggesting that the BFP peptide is able to induce an upregulation of ALP, which correlates with the first checkpoint for osteogenic differentiation.

Concomitantly, calcium deposition, an indication of osteogenesis at late stages of differentiation, was also evaluated using ARS staining. At 28 d, the hiPSCs cultured on the pure VN peptide-decorated surface (VN₁₀-TCP) form small numbers of bone nodules. Similar to the case for ALP activity, after combining with the BFP peptide, the osteogenic efficiency is greatly enhanced, which is reflected by the greater amounts and larger size of mineralization nodes compared with the VN₁₀-TCP groups. Therefore, BFP peptide may exert a synergistic effect in promoting osteogenesis combined with the traditional osteogenic factors (β -GP, AA, and Dex) in cell media. Additionally, more intensively distributed and bigger bone nodules are observed on the VN₅/BFP₅-TCP surface. Nevertheless, nearly no nodules are found on the VN₂/BFP₈-TCP surface which has the lowest number of cells. These results are also supported by the quantification of the calcium deposition (Figure 8a), which exhibits that cells on the VN₅/BFP₅-TCP group produce a larger number of calcium nodules. The results of ARS staining demonstrate the long-term stimulating effect of the presence of BFP peptide on the ability of hiPSCs to engage in osteo-differentiation processes.

Initialization and completion of cell differentiation are accompanied by regulation of the expression of multiple genes. The hiPSCs that are cultured on the VN₁₀-TCP surface in the mTeSR1 medium (Control) show unaltered pluripotent gene expression at each time interval with high expression of OCT-4 and Nanog makers and no expression of osteogenic makers, indicating that pluripotency is

maintained. Whereas, RT-PCR analysis reveals that pluripotency-associated genes (OCT-4, Nanog) are downregulated and these osteogenesis-related genes (RunX2, Col1a1, OPN, OCN) are upregulated in all groups subjected to osteoinductive medium, and their values are a function of culture time. After being cultured in osteoinductive medium, the expressions of OCT-4 and Nanog decrease sharply to near zero after 21 d, which implies that the pluripotency of hiPSCs is totally lost after 14 d. Runx2 is the early and master transcription factor initiating the osteogenic lineage transcriptional program,^[31] and OCN and Col1a1 are markers of the mineralization and production of the organic bone matrix, respectively.^[32] Osteopontin (OPN), one of the most abundant non-collagenous proteins of the bone matrix, plays a key role in the process of bone mineralization.^[33] The information presented in **Figure 9**, shows that cells that have been cultured in the VN₅/BFP₅-TCP and VN₈/BFP₂-TCP groups express more osteogenesis-related genes those that on VN₁₀-TCP and VN₂/BFP₈-TCP groups. In most cases, the fold change in Col1a1, OCN, OPN expression on VN₅/BFP₅-TCP substrates is greater than that on the VN₈/BFP₂-TCP surfaces at 14 and 21 d. BFP-1 peptide derived from the immature region of the BMP-7 protein has similar osteogenic inducing properties and may bind to the same functional sites (BMP receptors), triggering the upregulation of target osteogenic genes through Smads or mitogen-activated protein kinase (MAPK).^[34] The presented results provide ample evidence to confirm that the BFP-1 peptide significantly contributes to the osteogenic potential of the hiPSCs.

To further corroborate the results from the RT-PCR analysis, the expression of some osteospecific proteins including ALP, OPN, Col1a1, and OCN proteins was also probed at predefined times (**Figure 10**). Immunofluorescence staining results shows that the expression of four proteins in the VN₈/BFP₂-TCP group is higher than that present in the VN₁₀-TCP groups, corresponding to the findings from the gene analysis. When the VN/BFP ratio was 5:5, the production of these osteo-specific proteins is further enhanced. However, if the amount of BFP continued to increase, the production of each protein decreases significantly, which verifies the hypothesis that a very large BFP concentration is not enough to support hiPSCs survival, resulting in poor osteogenic efficiency. Overall, our current data for osteogenic differentiation experiments support the conclusion that VN₅/BFP₅-TCP greatly improves the osteogenic conversion of hiPSCs to osteoblast-like cells, subsequently resulting in the acceleration of osteogenesis.

According to the previous discussion, the proposed osteogenic conversion process of hiPSCs on the surfaces that had been co-decorated with dual VN/BFP peptides is summarized in **Figure 11**. After the hiPSCs grow to reach confluence on the surfaces, the mTeSR1 medium is altered to osteoinductive medium for osteogenic stimuli. At 4 d, the colonial morphology of hiPSCs changes to spindle shapes in the form of single cells, accompanied with a reduction in ALP activity. Morphological changes are one of the early indicators of differentiation. During 4–14 d, ALP expression is enhanced and filamentous F-actin appeared, indicating that osteogenic activation has been activated. According to the RT-PCR and immunofluorescence analysis, hiPSCs upregulate some osteospecific proteins

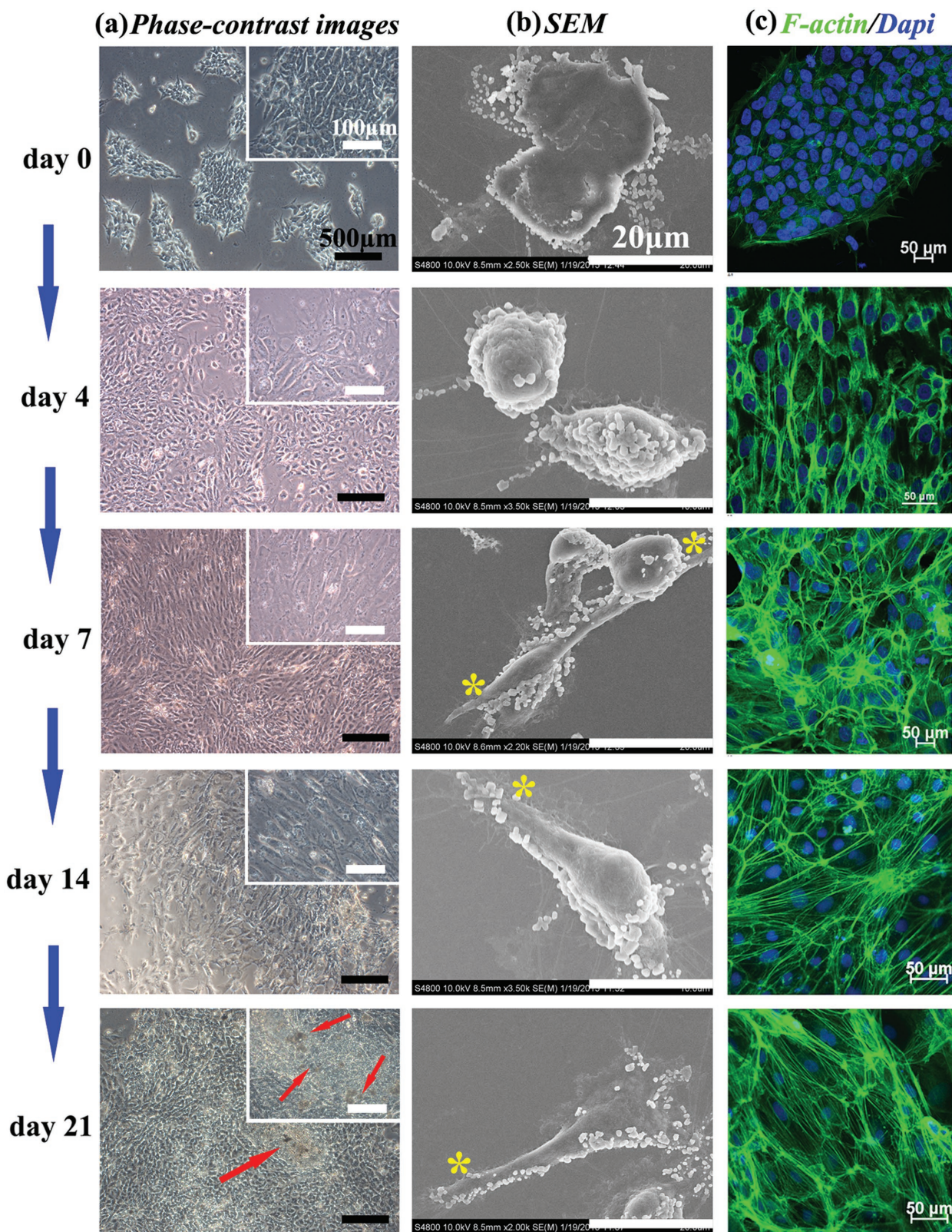


Figure 7. Alteration of the morphologies cytoskeletons of hiPSCs during osteogenic differentiation on the VN-CMC-TCP surfaces: a) Phase-contrast images, b) SEM observations, and c) fluorescence micrographs of F-actin cytoskeletal organization (green, labeled with FITC-phalloidin, counter-stained with DAPI for the nuclei in blue). Red arrows point to the formed nodules after 21 d of osteogenic induction. Asterisks (*) point to the filopodia of the differentiated cells that adhered to the substrates.

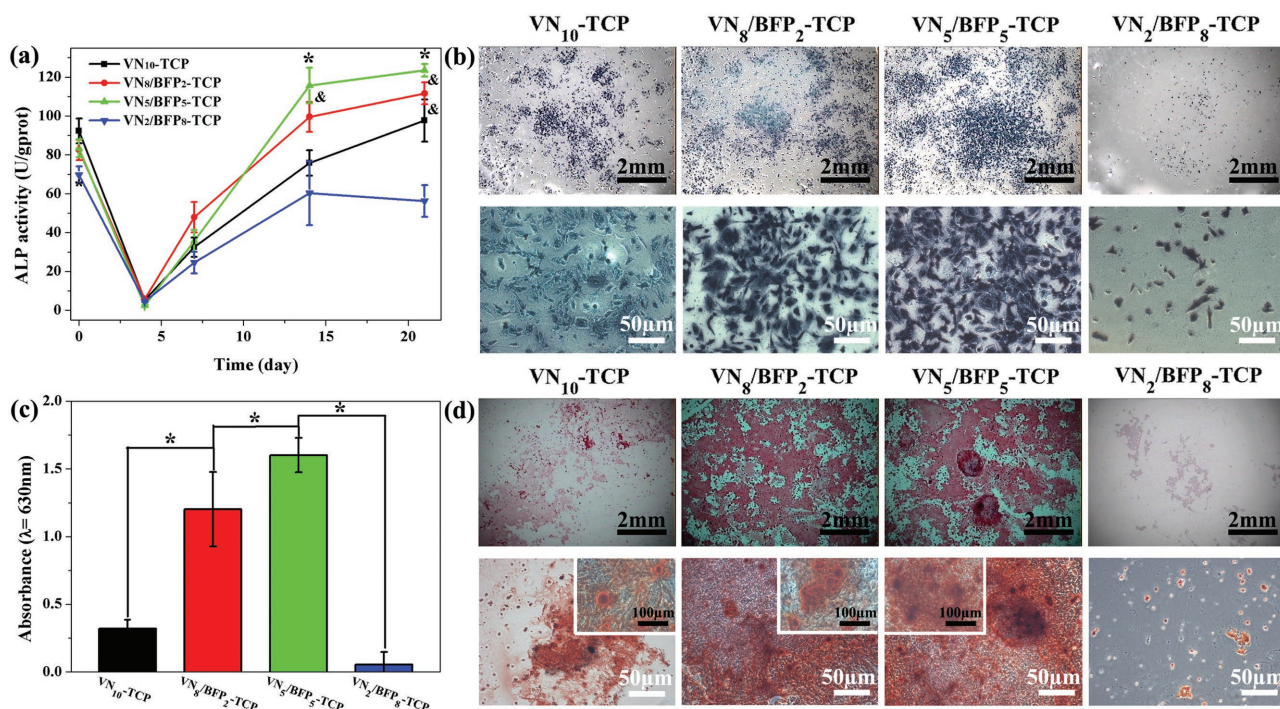


Figure 8. ALP expression of hiPSCs and calcium deposition on surfaces co-decorated with different peptides under osteoinductive conditions: a) quantification of ALP activity, b) representative images of ALP staining at 21 d, and c) quantification of calcium production, d) representative images of ARS staining at 28 d. *: $p < 0.05$ versus other groups, &: $p < 0.05$ versus VN_2/BFP_8 -TCP groups.

including OCN and Col1a1 at 21 d. After 28 d of osteogenic induction, a large number of calcium nodules are observed on the surfaces co-decorated with dual VN/BFP peptides, reflecting that the differentiated cells are at the late stage of osteogenic differentiation and produce mineralized ECM, which is a typical characteristic of osteoblast-like cells.

3. Conclusion

In summary, multipurpose peptide-grafted hydrogel surfaces have been successfully developed via grafting dual functional oligopeptides. These surfaces have been shown to support the expansion of hiPSCs along with their long-term maintenance,

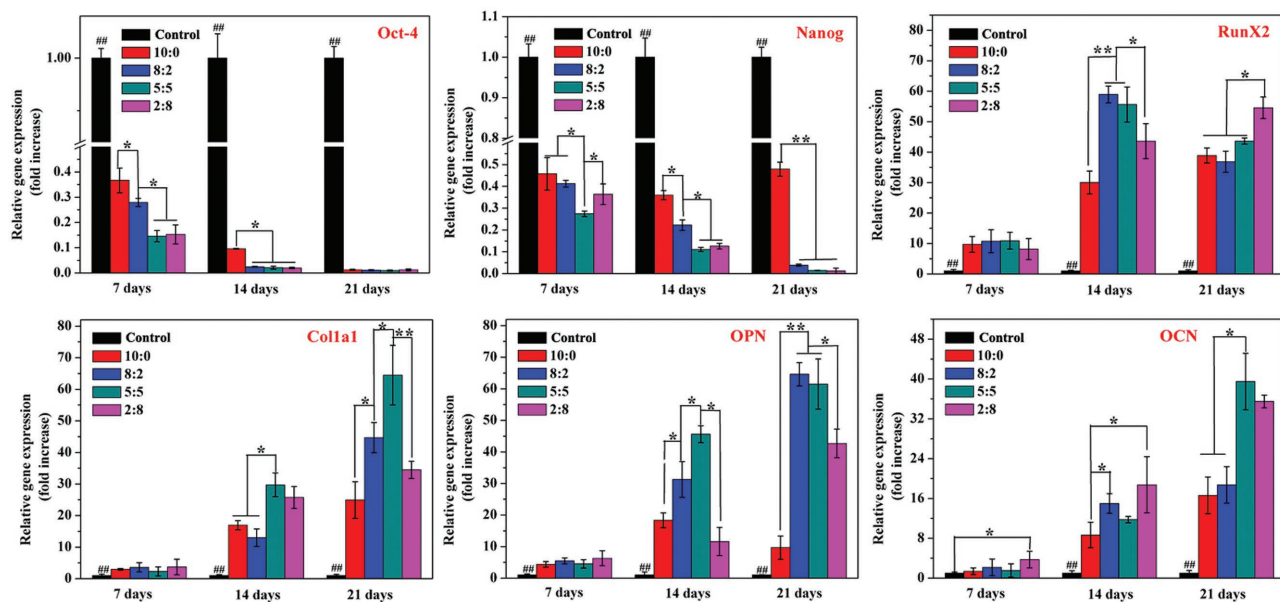


Figure 9. Real-time PCR detection of osteogenesis-related gene expressions (Oct-4, Nanog, Runx2, Col1a1, OPN, and OCN) of hiPSCs incubated on the dual VN/BFP peptides co-decorated samples at 7, 14, and 21 d; *: $p < 0.05$ and **: $p < 0.01$ between two groups, #: $p < 0.05$ and ##: $p < 0.01$ versus other groups.

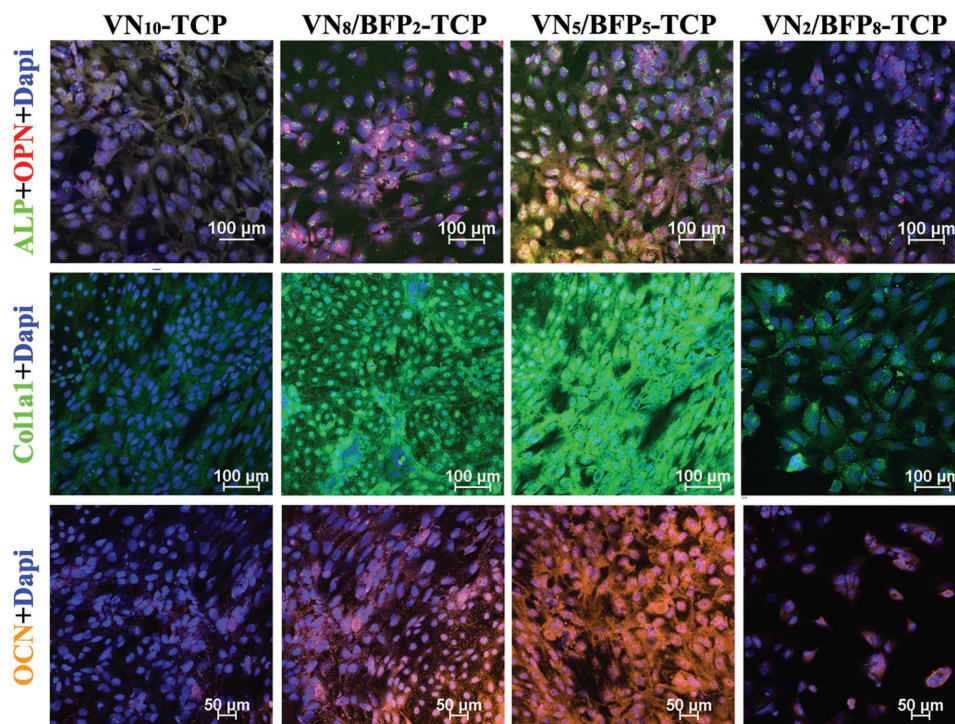


Figure 10. Immunocytochemical images of osteogenesis-related markers including ALP (green, at 21 d), OPN (red, at 21 d), Col1a1 (green, at 21 d), and OCN (yellow, at 28 d) expressed by hiPSCs cultured on the substrates that had been co-decorated with different dual peptides in osteoinductive media. Nuclei are visualized by Dapi-staining (blue). Scale bars: 100 μm .

and induce osteogenic differentiation of stem cells. The hiPSCs are able to proliferate and retain their pluripotency on the VN peptide-displaying substrates for two months (approximately ten passages) under a chemically defined condition (mTeSR1) without animal derived matrices, indicating the potential for production of clinical grade hiPSCs. These experimental results associated with an evaluation of surface engineering including cellular morphology observation, the ALP activity test, RT-PCR analysis and alizarin red staining all disclose that the surfaces

that had been modified with dual peptides facilitate osteogenic conversion of hiPSCs. In addition, various differentiated hiPSCs with different degrees of osteogenic differentiation can be achieved by altering the VN/BFP concentration ratio on the surface. The method is facile, cost-effective, and practical, while it has the additional merits of eradicating risks of viral and microbial contamination picked up from animal derived proteins. Future studies will need to investigate the in vivo bone formation capability induced by the transplantation of

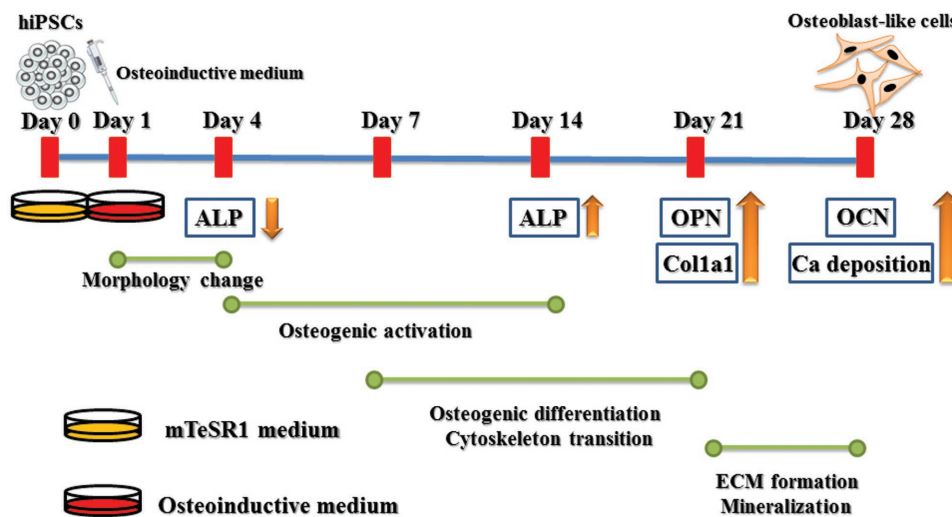


Figure 11. The proposed osteogenic conversion process for hiPSCs on the hydrogel surfaces that had been co-decorated with dual VN/BFP peptides.

the hPSCs with dual peptides co-decorated matrices. The well-defined, xeno-free and engineered surfaces, that support culture and manipulate/hasten osteoblastic maturation of hiPSCs, have great promise for bone regenerative medicine and tissue engineering. This study also offers a promising strategy for obtaining other tissue-specific cells (such as neuron/neurocyte-like, and hepatocyte-like, and cardiomyocyte-like cells) from hiPSCs with immobilization of other bioactive ligands.

4. Experimental Section

Preparation of VN Peptide-Grafted Hydrogel Surface: The 6-well TCP (Corning, USA) were firstly exposed in an ultraviolet/ozone condition (UV, $\lambda = 232$ nm, 100 mW cm⁻²) for 5 min using a compact microprocessor controlled UV flood curing system (INTELLI-RAY 400, Uvitron, USA). Whereafter, they were promptly immersed in a 5 mL per well of 3% (w/v) CMC solution ($M_w \approx 9.5$ – 20.9 kDa, Aladdin, Shanghai, China) for another 24 h at 37 °C in a constant temperature shaker. The treated substrates were thoroughly rinsed with deionized water (D.I. water) to remove the physically absorbed CMC, and allowed to dry. The CMC-modified samples were preactivated by 2×10^{-3} M N-(3-(Dimethylamino)propyl)-EDS (Aladdin) and 5×10^{-3} M NHS (Aladdin) in 0.1 M 2-(N-morpho)ethanesulfonic acid (MES, Aladdin) buffer (pH = 5.6) for 40 min to form hydrogel on the surface, which were denoted as CMC–TCP. To facilitate chemical conjugation onto the material surfaces, the peptide was modified at its N-terminal with a lysine-containing spacer. After rinsing with D.I. water, 500 μ L of 1×10^{-3} M VN peptide (Ac-KGGPQVTRGDVFTMP, Chinapeptides Co., Ltd., Shanghai, China, >99% purity) was pipetted to each of the carboxyl-rich CMC–TCP hydrogel surfaces and incubated at 4 °C overnight. These samples were referred as VN–CMC–TCP. The resulting peptide-grafted plates were washed with D.I. water to remove the unattached peptide, and dried before characterization and cell experiments.

Surface Characterization: TCPs before and after CMC/peptide modifications were analyzed by ATR-FTIR, XPS, contact angle goniometry, SEM, as well as AFM. ATR-FTIR spectra (Magna-IR 750, Nicolet, USA) were collected to analyze the functional groups of substrates in the range of 400–4000 cm⁻¹. Chemical composition was analyzed by XPS (AXIS Ultra, Kratos Analytical Ltd., UK) for both survey and high-resolution spectra. The binding energies were calibrated using a C 1s hydrocarbon peak at ≈ 285 eV; and the quantitative analysis and curve fitting were conducted using the CasaXPS software. The hydrophilicity/hydrophobicity was measured by contact angle goniometry with a Dataphysics OCA20 contact angle system (Germany) at ambient temperature based on the sessile drop method. Six parallel specimens were used to provide an average and standard deviation. In addition, surface morphology and roughness of the treated substrates was characterized by a field emission SEM (JSM-6701F, JEOL, Japan) and AFM (Dimension ICON, Bruker, USA). Each sample was tested at random locations in sextuplicates to improve the statistical rigor of the AFM results.

To evaluate the adhesion strength between the hydrogel coating and TCP substrate, a Nano Indenter System (Hysitron, USA) was used to measure nano-scratch resistance with a spherical diamond Rockwell indenter. The tip approached and was loaded into the coating with an increasing rate of 30 μ N s⁻¹ up to 1000 μ N, making a 10 μ m scratch at the prescribed direction. The initiation of the first crack detected by the acoustic sensor was associated with the critical load, and was related to the adhesion strength of the hydrogel coating. The tests were performed in a clean environment at 25 °C. For statistical purposes, at least six parallel results were deemed valid, and average values were calculated from these results.

hiPSCs Culture: The hiPSCs (hNF-C1 line, provided by Chinese Academy of Sciences, China) were generated from human skin fibroblasts by retroviral introduction of four Yamanaka's factors: Oct3/4, Sox2, Klf4, and c-Myc. These hiPSCs were cultured on Matrigel-coated plates using chemically defined mTeSR1 medium (StemCell Technologies, Canada) containing 55×10^{-6} M Rock inhibitor (Y-27632, Selleck Chemicals, USA), and 1% (v/v) penicillin/streptomycin (Invitrogen, USA) at 37 °C in a

humidified 5% CO₂ incubator (HERAcell 150i, Thermo Fisher, USA). Cells between 30 and 50 times of passages were used for in vitro experiments. Cells were fed daily and passaged at a 1:3 splitting ratio every 3–4 d by exposure to 0.5×10^{-3} M EDTA (Aladdin) for 4–5 min at 37 °C. Prior to cell experiments, the studied substrates were sterilized with 75% ethanol for 1 h, followed by a thorough rinse with disinfected PBS buffer.

Peptide Density Assessment and Cell Attachment on VN Peptide-Grafted Hydrogel Surface: In order to prepare various CMC–TCP substrates, different concentrations of CMC solutions (0, 1, 3, 5, and 10% (wt/v) and 1×10^{-3} M VN peptide were used, while the other synthetic parameters and procedures were maintained the same as described above. On the other hand, a dilution series of VN peptide solutions (0.25, 0.5, 0.75, 1, and 1.25×10^{-3} M) with a volume of 1 mL were, respectively, pipetted into each activated 3% (wt/v) CMC modified TCP overnight at 4 °C to fabricate VN–CMC–TCP hydrogels with various peptide amounts. To track the change in conjugated peptide surface content, FITC-labeled VN peptide (Chinapeptides) solution was used to supersede VN peptide. The quantitative average fluorescence intensity of the surfaces was acquired using a Multilabel Reader (2300, Perkin Elmer, Singapore) with an absorbed wavelength of 488 nm and an emitted wavelength of 525 nm. Six independent measurements were performed for each surface. The real peptide density on each surface was calculated based on the established standard peptide density calibration curves.

hNF-C1hiPSCs were applied to investigate the influence of CMC and peptide concentrations on the adhesion and cellular morphology of hiPSCs in mTeSR1 medium. After rinsing with DMEM/F12 (Gibco, USA) three times, cells were harvested, counted, and seeded on the VN peptide-grafted surfaces at a density of 1.5×10^5 cells per mL, and Matrigel-coated plates were prepared and used as control. The cell viability of hiPSCs on the samples was evaluated using a cell counting assay kit-8 (CCK-8, Dojindo, Japan). After 1 d of culture, the CCK-8 solution was added into each well at a proportion of 1:10 (v/v) after a 2 h incubation in the dark. Then 100 μ L of supernatant from each well was transferred to new 96-well plates. The absorbance value of the supernatant optical density value was measured with a microplate reader (model 680, Bio-Rad, Canada) at the 450 nm wavelength. Six parallel specimens were used to provide an average and standard deviation for each group. An inverted phase-contrast microscope (Nikon Eclipse TS100, Japan) was employed to observe the adhesion of the cells.

Long-Term Culture of hiPSCs on VN Peptide-Grafted Hydrogel Surface: After reaching 80–90% confluence, the cells on Matrigel were harvested by EDTA, directly seeded onto 6-well VN–CMC–TCP surfaces, then were fed daily with mTeSR1 medium containing 5×10^{-6} M Y-27632 and 1% penicillin/streptomycin. Differentiated cells were marked and removed mechanically by a negative pressure aspirator. Depending on size and density of colonies, cells were passaged every 3–5 d at a ratio of 1:3 onto new VN–CMC–TCP hydrogel surfaces. hiPSCs were serially passaged on VN–CMC–TCP surfaces for ten passages under the same conditions. Cells cultured on the Matrigel-coated plates were used as a control. The morphology of the cells at each passage was observed using the inverted microscope.

Identification of cell Pluripotency on VN Peptide-Grafted Hydrogel Surface—Cell Proliferation: The proliferation of hiPSC during 5 d at passage 1 (p1), passage 5 (p5), and passage 10 (p10) on the VN–CMC–TCP hydrogel and Matrigel surfaces was also assessed through CCK-8. Six parallel specimens were used to provide an average and standard deviation for each group.

Identification of cell Pluripotency on VN Peptide-Grafted Hydrogel Surface—Immunocytochemistry for Pluripotency Markers: The hiPSCs cultured on the hydrogel surface at p1, p5, and p10 were subjected to immunocytochemical analysis. The cells were fixed using 4% paraformaldehyde and permeabilized with 0.1% Triton X-100 for 10 min. Afterward, they were incubated with 1% bovine serum albumin/PBS buffer at 37 °C for 30 min to block nonspecific binding. Then, cells were incubated with diluent primary antibodies including Mouse Anti-Nanog IgG to Human (1:400, Cell Signaling Technology, CST, USA), Rabbit Anti-Oct-4 IgG to Human (1:1000, CST), Mouse Anti-SSEA-3 IgG to Human (1:400, Santa Cruz, USA), and Rabbit Anti-SSEA-4 IgG to Human (1:400, Santa Cruz), and Mouse Anti-Tra-1-60 IgG to Human

(1:200, Santa Cruz) at 4 °C overnight. Next day, the cells were incubated with corresponding secondary antibodies (FITC-488 goat antirabbit or TRITC-543 goat antimouse, ZSGB-BIO, Beijing, China) diluted in PBS at a ratio of 1:100 in the dark for 1 h at ambient temperature. Finally, cell nuclei were stained with 10 µg mL⁻¹ Dapi (Roche, Germany) for 5 min. Each staining step was followed by three washes in PBS buffer. The expression of these biomarkers was visualized immediately under a confocal laser scanning microscopy (CLSM, A1R-si, Nikon, Japan).

Identification of cell Pluripotency on VN Peptide-Grafted Hydrogel Surface—RNA Isolation and Quantitative Real-time PCR Analysis: Total mRNA was extracted from cells using TRIzol (Invitrogen, USA) and reverse transcribed into cDNA by means of a Revert Aid First Stand cDNA Synthesis Kit (Thermo Fisher) as per the manufacturer's instructions. Then, quantitative RT-PCR analysis was conducted with SYBR Green I (Roche, USA) using an ABI 7500 RT-PCR machine (Applied Biosystems, USA). All experiments were performed in triplicate, and the expression of glyceraldehyde-3-phosphate dehydrogenase was assigned as an endogenous control. The primers (provided from Sangon Biotech, Shanghai, China) used in the present study were listed in Table S1 in the Supporting Information. The thermal profile of the PCR was 50 °C for 2 min and 95 °C for 10 min, followed by 40 cycles at 95 °C for 5 s and 60 °C for 1 min. The comparative CT (2^{-ΔΔCt}) method was employed to evaluate fold differences in gene expression between groups.

Identification of cell Pluripotency on VN Peptide-Grafted Hydrogel Surface—Flow Cytometry Analysis: hiPSCs cultured on VN-CMC-TCP hydrogel and Matrigel surfaces were dissociated into single cells by treatment with 0.25% Trypsin/EDTA (StemCell Technologies) for 4 min at 37 °C when grown to 90% confluence. The cells were pelleted by centrifugation at 200 g and then re-suspended in 1 mL of the FACS buffer (Solarbio). For the flow cytometry assay of Oct-4, cells were treated with 200 µL 90% formaldehyde solution on ice for 30 min. After this step, the cells were sequentially incubated with the primary antibodies (Mouse Anti-Oct-4 Monoclonal Antibody, StemCell Technologies) and secondary antibodies (Goat Anti-Mouse Alexa Fluor 488 IgG, Invitrogen, USA) for 30 min 37 °C. The mouse IgG1 (StemCell Technologies) was utilized as the isotype control. For the flow cytometry measurement of Nanog, SSEA-3 and Tra-1-60, cells were incubated with PE-conjugated mouse monoclonal IgM antibody against human SSEA-3 (StemCell Technologies), PE-conjugated mouse polyclonal IgM antibody against human Nanog (Invitrogen) and PE-conjugated mouse monoclonal IgM antibody against human Tra-1 60 (StemCell Technologies), respectively, for 30 min at 37 °C. The mouse IgM (StemCell Technologies) was used as the isotype control. Cells were washed twice with FACS buffer after each step of permeability and staining. At a final step the cells were re-suspended in 600 µL of FACS buffer and immediately detected using a BD FACS Calibur System (LSRFortessa, USA), before the data was analyzed using Flowjo Software. In the first ten passages of hiPSCs on the VN-CMC-TCP hydrogel and Matrigel surfaces, the expression of intracellular markers Oct-4 and that of surface markers SSEA-3 at each passage were evaluated using flow cytometry.

Identification of cell Pluripotency on VN Peptide-Grafted Hydrogel Surface—Karyotyping: After culturing on the VN peptide-grafted hydrogel surfaces at p1, p5, and p10, hiPSCs were transferred back onto the Matrigel surfaces for karyotyping analysis. Cell samples were submitted to the College of Life Sciences, Sichuan University for karyotyping analysis using a standard G banding technique. A minimum of 20 metaphase spreads were analyzed, and an additional 20 were counted. The final karyotype was recorded if it was present in more than 85% of the samples.

Preparation of the Hydrogel Surfaces co-Decorated with the Dual VN/BFP Peptides: VN and BFP (Ac-KGGQGFSYPYKAVFSTQ, Chinapeptides, >99% purity) peptides were dissolved in sterilized PBS with a concentration of 1 × 10⁻³ M, separately, and then two peptide were mixed in various volume ratios (VN:BFP = 10:0, 8:2, 5:5, and 2:8). The hydrogel surfaces co-decorated with the VN/BFP peptides were fabricated as described above in section "2.1 Preparation of VN peptide-grafted hydrogel surface". Peptides co-decorated TCP substrates were named VN₁₀-TCP, VN₈/BFP₂-TCP, VN₅/BFP₅-TCP, VN₂/BFP₈-TCP, respectively, according to the volume ratios of VN/BFP.

To quantify the peptide immobilized at different volume ratios, the FITC-labeled VN peptide and Rhodamine-labeled BFP-1 peptide (Chinapeptides) were anchored onto the CMC-TCP surfaces to obtain a standard calibration curve of fluorescence intensity. The qualitative intensity and distribution of fluorescence on the surfaces were detected using inverted fluorescent microscopy. Furthermore, the quantitative average fluorescence intensity of the VN/BFP co-decorated surfaces was also determined using a Multilabel Reader. Six independent measurements were performed for each surface.

Osteogenic Induction: The osteoinductive medium was comprised of fresh low-glucose DMEM containing 10% fetal bovine serum (FBS, Gibco), 1% penicillin/streptomycin (Invitrogen), 50 µg mL⁻¹ ascorbic acid (Sigma-Aldrich), 10 × 10⁻³ M sodium β-glycerophosphate (Sigma-Aldrich), and 100 × 10⁻⁹ M dexamethasone (Sigma-Aldrich). hiPSCs were first attached to the different VN/BFP co-decorated substrates in mTeSR1 medium for 3 d. Afterward, the culture medium was replaced by an osteoinductive medium. The culture medium was refreshed every day, and the whole process lasted for 28 d.

Osteogenic Differentiation Evaluation—Cell Morphology and Cytoskeleton Observation: Cellular distribution, growth, and morphology along with features of the cytoskeleton of hiPSCs during osteogenic induction were evaluated using the optical microscope, SEM and F-actin fluorescence staining. After different induction times, the cells were observed using an inverted microscope. Then they were fixed in 2.5% glutaraldehyde, dehydrated with graded ethanol solutions, and dried for SEM observation. The rinsed cells were fixed with 4% paraformaldehyde, permeabilized with 0.1% Triton X-100 (Sigma-Aldrich) for 5 min, followed by adding 1 µg mL⁻¹ FITC-phalloidin (Sigma-Aldrich) to stain cells for 30 min. After washing with PBS, samples were incubated for 10 min with 10 µg mL⁻¹ DAPI (Sigma-Aldrich), and viewed using CLSM.

Osteogenic Differentiation Evaluation—ALP Activity: ALP activity of hiPSCs on samples was quantified using an ALP assay reagent kit (Nanjing Jiancheng Bioengineering Institute, China). At different times, the hiPSCs were lysed, and 30 µL of cell lysates were mixed with the ALP assay working solution and assayed following the manufacturer's instructions. For normalization, the total protein concentration was measured using a bicinchoninic acid protein assay kit (Thermo Fisher). Thus, the ALP activity was normalized and expressed as the total protein content (U g_{prot}⁻¹). Six replicate specimens were tested for each group at each incubation period. Simultaneously, EHC staining was also performed to visualize the ALP distribution and expression on samples using a BCIP/NBT ALP staining kit (Beijing ComWin Biotech, China).

Osteogenic Differentiation Evaluation—Alizarin Red Staining: Calcium mineralization was evaluated at 28 d through staining using a Alizarin Red S (ARS) solution (Sigma-Aldrich). Cells layers were fixed with 4% paraformaldehyde for 15 min before being immersed in ARS solution (2%, pH 4.2) for 30 min. After thorough washing with D.I. water, the newly formed bone-like nodules on the materials were captured using a scanner. To further quantify calcium mineralization, the ARS-stained samples were incubated using cetylpyridinium chloride solution (100 × 10⁻³ M, Sigma-Aldrich) at 37 °C for 24 h with shaking to solubilize calcium mineral. The absorbance of eluate was determined at 550 nm using the microplate reader. Six specimens were tested for each group.

Osteogenic Differentiation Evaluation—RNA Extraction and RT-PCR: After 7, 14, and 21 d of osteoinduction, the total mRNA was isolated, and RT-PCR analysis was conducted as described above. Primers for the osteogenic differentiation test were listed in Table S2 in the Supporting Information.

Osteogenic Differentiation Evaluation—Immunofluorescence Staining for Osteo-Specific Markers: At the predetermined time intervals, after fixation, the cells were permeabilized, and treated with 1% BSA/PBST solution, before being incubated with primary antibodies against ALP (1:400, CST), OPN (1:400, CST), Col1a1 (1:400, CST), and OCN (1:400, CST) at 4 °C overnight. Next day, cells were incubated with the FITC-488 goat anti-rabbit (1:100) or TRITC-543 goat anti-mouse (1:100) secondary antibodies for 1 h at room temperature in the dark. Finally, the cells were counter-stained with DAPI (10 µg mL⁻¹) for identification of cell nuclei and immediately viewed by the CLSM.

Statistical Analysis: All data was expressed as a mean \pm standard deviation. One-way analysis of variance and Tukey's post hoc tests were used to determine the significant differences among the groups, and *p* values < 0.05 were considered indicative of statistical significance.

Supporting Information

Supporting Information is available from the Wiley Online Library or from the author.

Acknowledgements

This work was jointly supported by the National Natural Science Foundation of China (No. 81571824), Peking University's 985 Grant, the financial support by the Science and Technology Program of Sichuan Province (2017FZ0046), Project Funded by China Postdoctoral Science foundation (2017M610600), Full-time Postdoctoral Research Fund of Sichuan University (2017SCU12016), Research Program of Star of Chemical Engineering (School of Chemical Engineering, Sichuan University), and Australian Research Council. ZGC thanks the USQ Start-up Grant and Strategic Research Funds. MD would like to acknowledge the support of the ARC Research Hub for Advanced Manufacturing of Medical Devices. The affiliations were updated on March 14, 2018, following initial publication on early view.

Conflict of Interest

The authors declare no conflict of interest.

Keywords

engineered surfaces, expansion, functional peptides, hiPSCs, osteoblastic maturation

Received: September 24, 2017

Revised: November 22, 2017

Published online: January 17, 2018

- [1] a) T. J. Nelson, A. Martinezfernandez, A. Terzic, *Nat. Rev. Cardiol.* **2010**, *7*, 700; b) G. Amabile, A. Meissner, *Trends Mol. Med.* **2009**, *15*, 59; c) K. Takahashi, S. Yamanaka, *Cell* **2006**, *126*, 663.
- [2] J. Yu, M. A. Vodyanik, K. Smuga-Otto, J. Antosiewicz-Bourget, J. L. Frane, S. Tian, J. Nie, G. A. Jonsdottir, V. Ruotti, R. Stewart, *Stem Cell Rev.* **2007**, *8*, 693.
- [3] O. Genbacev, A. Krtolica, T. Zdravkovic, E. Brunette, S. Powell, A. Nath, E. Caceres, M. McMaster, S. McDonagh, Y. Li, *Fertil. Steril.* **2005**, *83*, 1517.
- [4] O. Hovatta, M. Mikkola, K. Gertow, A. M. Strömberg, J. Inzunza, J. Hreinsson, B. R. Rozell, E. Blennow, M. Andäng, L. Åhrlund-Richter, *Hum. Reprod.* **2003**, *18*, 1404.
- [5] C. Xu, M. S. Inokuma, J. Denham, K. Golds, P. Kundu, J. D. Gold, M. K. Carpenter, *Nat. Biotechnol.* **2001**, *19*, 971.
- [6] a) A. Higuchi, Q. D. Ling, Y. A. Ko, Y. Chang, A. Umezawa, *Chem. Rev.* **2011**, *111*, 3021; b) Y. Deng, X. Zhang, X. Zhao, Q. Li, Z. Ye, Z. Li, Y. Liu, Y. Zhou, H. Ma, G. Pan, *Acta Biomater.* **2013**, *9*, 8840.
- [7] a) T. J. Rowland, L. M. Miller, A. J. Blaschke, E. L. Doss, A. J. Bonham, S. T. Hikita, L. V. Johnson, D. O. Clegg, *Stem Cells Dev.* **2009**, *19*, 1231; b) S. R. Braam, L. Zeinstra, S. Litjens, D. Ward-Van Oostwaard, V. D. B. Stieneke, L. Van Laake, F. Lebrin, P. Kats, R. Hochstenbach, R. Passier, *Stem Cells* **2008**, *26*, 2257.
- [8] a) S. Rodin, A. Domogatskaya, S. Ström, E. M. Hansson, K. R. Chien, J. Inzunza, O. Hovatta, K. Tryggvason, *Nat. Biotechnol.* **2010**, *28*, 611; b) S. Rodin, L. Antonsson, O. Hovatta, K. Tryggvason, *Nat. Protoc.* **2014**, *9*, 2354.
- [9] Y. Hayashi, T. Chan, M. Warashina, M. Fukuda, T. Ariuzumi, K. Okabayashi, N. Takayama, M. Otsu, K. Eto, M. K. Furue, *PLoS One* **2010**, *5*, e14099.
- [10] T. Miyazaki, S. Futaki, H. Suemori, Y. Taniguchi, M. Yamada, M. Kawasaki, M. Hayashi, H. Kumagai, N. Nakatsuji, K. Sekiguchi, *Nat. Commun.* **2012**, *3*, 1236.
- [11] S. A. Duncan, A. Toshihiro, S. T. Karim, N. Masato, *BMC Dev. Biol.* **2010**, *10*, 60.
- [12] a) K. Yang, J. Lee, S. W. Cho, *Int. J. Stem Cells* **2012**, *5*, 1; b) B. S. Mallon, K. Y. Park, K. G. Chen, R. S. Hamilton, R. D. Mckay, *Int. J. Biochem. Cell Biol.* **2006**, *38*, 1063.
- [13] J. M. Karp, L. S. Ferreira, A. Khademhosseini, A. H. Kwon, J. Yeh, S. L. P. D. Robert, *Stem Cells* **2006**, *24*, 835.
- [14] L. A. Smith, X. Liu, J. Hu, P. X. Ma, *Biomaterials* **2010**, *31*, 5526.
- [15] A. Ardeshirylajimi, S. Hosseinkhani, K. Parivar, P. Yaghmaei, M. Soleimani, *Mol. Biol. Rep.* **2013**, *40*, 4287.
- [16] a) A. Higuchi, S. S. Kumar, Q. D. Ling, A. A. Alarfaj, M. A. Munusamy, K. Murugan, S. T. Hsu, G. Benelli, A. Umezawa, *Prog. Polym. Sci.* **2017**, *65*, 83; b) A. Higuchi, Q. D. Ling, S. S. Kumar, M. Munusamy, A. A. Alarfaj, A. Umezawa, G. J. Wu, *Prog. Polym. Sci.* **2014**, *39*, 1348.
- [17] a) H. Kang, C. Wen, Y. Hwang, Y. R. Shih, M. Kar, S. W. Seo, S. Varghese, *J. Mater. Chem. B* **2014**, *2*, 5676; b) K. Rutledge, Q. Cheng, M. Pryzhkova, G. M. Harris, E. Jabbarzadeh, *Tissue Eng. Part C Methods* **2014**, *20*, 865.
- [18] a) Z. Melkounian, J. L. Weber, D. M. Weber, A. G. Fadeev, Y. Zhou, P. Dolleysonneville, J. Yang, L. Qiu, C. A. Priest, C. Shogbon, *Nat. Biotechnol.* **2010**, *28*, 606; b) H. J. Park, K. Yang, M. J. Kim, J. Jang, M. Lee, D. W. Kim, H. Lee, S. W. Cho, *Biomaterials* **2015**, *50*, 127; c) J. R. Klim, L. Li, P. J. Wrighton, M. S. Piekarczyk, L. L. Kiessling, *Nat. Methods* **2010**, *7*, 989; d) Y. Deng, Y. Yang, S. Wei, *Biomacromolecules* **2017**, *18*, 587.
- [19] D. A. Brafman, C. W. Chang, A. Fernandez, K. Willert, S. Varghese, S. Chien, *Biomaterials* **2010**, *31*, 9135.
- [20] a) H. K. Kim, J. H. Kim, D. S. Park, K. S. Park, S. S. Kang, J. S. Lee, M. H. Jeong, T. R. Yoon, *Biomaterials* **2012**, *33*, 7057; b) Y. J. Lee, J. H. Lee, H. J. Cho, H. K. Kim, T. R. Yoon, H. Shin, *Biomaterials* **2013**, *34*, 5059.
- [21] M. Wang, Y. Deng, P. Zhou, Z. Luo, Q. Li, B. Xie, X. Zhang, T. Chen, D. Pei, Z. Tang, *ACS Appl. Mater. Interfaces* **2015**, *7*, 4560.
- [22] a) D. Bhattacharya, M. Das, D. Mishra, I. Banerjee, S. K. Sahu, T. K. Maiti, P. Pramanik, *Nanoscale* **2011**, *3*, 1653; b) R. N. Chen, G. M. Wang, C. H. Chen, H. O. Ho, M. T. Sheu, *Biomacromolecules* **2006**, *7*, 1058; c) R. Jayakumar, M. Prabaharan, S. V. Nair, S. Tokura, H. Tamura, N. Selvamurugan, *Prog. Mater. Sci.* **2010**, *55*, 675.
- [23] a) R. Budiraharjo, K. G. Neoh, E. T. Kang, *J. Colloid Interface Sci.* **2012**, *366*, 224; b) D. Mishra, B. Bhunia, I. Banerjee, P. Datta, S. Dhara, T. K. Maiti, *Mater. Sci. Eng. C Mater. Biol. Appl.* **2011**, *31*, 1295.
- [24] S. Chen, Y. Wu, F. Mi, Y. Lin, L. Yu, H. Sung, *J. Controlled Release* **2004**, *96*, 285.
- [25] Y. Sun, Y. Deng, Z. Ye, S. Liang, Z. Tang, S. Wei, *Colloids Surf. B Biointerfaces* **2013**, *111*, 107.
- [26] a) J. Liu, X. Liu, T. Xi, C.-C. Chu, *J. Mater. Chem. B* **2015**, *3*, 878; b) J. Liu, P. Wang, C. Chu, T. Xi, *J. Mater. Chem. B* **2017**, *5*, 1787.
- [27] Y. J. Li, E. H. Chung, R. T. Rodriguez, M. T. Firpo, K. E. Healy, *J. Biomed. Mater. Res. A* **2006**, *79A*, 1.
- [28] a) K. Watanabe, M. Ueno, D. Kamiya, A. Nishiyama, M. Matsumura, T. Wataya, J. B. Takahashi, S. Nishikawa, S. Nishikawa, K. Muguruma, *Nat. Biotechnol.* **2007**, *25*, 681; b) K. Gauthaman, C. Y. Fong, A. Bongso, *Stem Cell Rev.* **2010**, *6*, 86.

- [29] a) A. Sachar, T. A. Strom, M. J. Serrano, M. D. Benson, L. A. Opperman, K. K. H. Svoboda, X. Liu, *J. Biomed. Mater. Res. A* **2012**, 100A, 3029; b) Y. Bai, Y. Deng, Y. Zheng, Y. Li, R. Zhang, Y. Lv, Q. Zhao, S. Wei, *Mater. Sci. Eng. C Mater. Biol. Appl.* **2016**, 59, 565.
- [30] a) A. K. Gaharwar, S. M. Mihaila, A. Swami, A. Patel, S. Sant, R. L. Reis, A. P. Marques, M. E. Gomes, A. Khademhosseini, *Adv. Mater.* **2013**, 25, 3329; b) G. Kaur, M. T. Valarmathi, J. D. Potts, E. Jabbari, T. Sabo-Attwood, W. Qian, *Biomaterials* **2010**, 31, 1732.
- [31] a) H. Wu, T. W. Whitfield, J. A. Gordon, J. R. Dobson, P. W. Tai, A. J. van Wijnen, J. L. Stein, G. S. Stein, J. B. Lian, *Genome Biol.* **2014**, 15, R52; b) T. Komori, *J. Cell. Biochem.* **2011**, 112, 750.
- [32] a) C. M. Kaneto, P. S. Lima, D. L. Zanette, K. L. Prata, J. M. P. Neto, F. J. D. Paula, W. A. Silva Jr., *BMC Med. Genet.* **2014**, 15, 45; b) G. Kaur, M. T. Valarmathi, J. D. Potts, Q. Wang, *Biomaterials* **2008**, 29, 4074.
- [33] T. Uemura, A. Nemoto, Y. K. Liu, H. Kojima, J. Dong, T. Yabe, T. Yoshikawa, H. Ohgushi, T. Ushida, T. Tateishi, *Mater. Sci. Eng. C Mater. Biol. Appl.* **2001**, 17, 33.
- [34] a) A. Bandyopadhyay, P. S. Yadav, P. Prashar, *Biochem. Pharmacol.* **2013**, 85, 857; b) A. C. Carreira, F. H. Lojudice, E. Halcsik, R. D. Navarro, M. C. Sogayar, J. M. Granjeiro, *J. Dent. Res.* **2014**, 93, 335.